7240 *Biochemistry* **2009,** *48,* 7240–7250
DOI: 10.1021/bi900880c

BIOCHEMISTRY
including biophysical chemistry & molecular biology
Article

Nucleotide Binding and Allosteric Modulation of the Second AAA+ Domain of ClpB Probed by Transient Kinetic Studies[†]

Nicolas D. Werbeck, Julian N. Kellner, Thomas R. M. Barends, and Jochen Reinstein*

Max Planck Institute for Medical Research, Department of Biomolecular Mechanisms, Jahnstrasse 29, D-69120 Heidelberg, Germany

Received May 25, 2009; Revised Manuscript Received June 29, 2009

ABSTRACT: The bacterial AAA+ chaperone ClpB provides thermotolerance by disaggregating aggregated proteins in collaboration with the DnaK chaperone system. Like many other AAA+ proteins, ClpB is believed to act as a biological motor converting the chemical energy of ATP into molecular motion. ClpB has two ATPase domains, NBD1 and NBD2, on one polypeptide chain. The functional unit of ClpB is a homohexameric ring, with a total of 12 potential nucleotide binding sites. Previously, two separate constructs, one each containing NBD1 or NBD2, have been shown to form a functional complex with chaperone activity when mixed. Here we aimed to elucidate the nucleotide binding properties of the ClpB complex using pre-steady state kinetics and fluorescent nucleotides. For this purpose, we first disassembled the complex and characterized in detail the binding kinetics of a construct comprising NBD2 and the C-terminal domain of ClpB. The monomeric construct bound nucleotides very tightly. ADP bound 2 orders of magnitude more tightly than ATP; this difference in binding affinity resulted almost exclusively from different dissociation rate constants. The nucleotide binding properties of NBD2 changed when this construct was complemented with a construct comprising NBD1 and the middle domain. Our approach shows how complex formation can influence the binding properties of the individual domains and allows us to assign nucleotide binding features of this highly complex, multimeric enzyme to specific domains.

The "ATPases associated with various cellular activities" (AAA+)[1] comprise a family of enzymes involved in a variety of processes in all living organisms. Most of the members of this family form multimeric ring structures which are the active units of many AAA+ proteins (*1*, *2*). These proteins participate in many important cellular processes such as DNA replication, protein degradation, and vesicle transport by coupling the chemical energy stored in ATP to conformational changes. This process involves a highly coordinated interplay of different domains on a protomer as well as different protomers within the multimeric ring. Among AAA+ proteins, there are members that contain one nucleotide binding domain per protomer (class II) and others with two (class I) (*3*). ClpB is a bacterial member of the AAA+ superfamily which provides thermotolerance by disaggregating protein aggregates, together with the DnaK chaperone system (*4*−*6*). ClpB and its homologue in yeast, Hsp104, form hexameric, ringlike structures which are considered to be the active units (*7*, *8*). With two nucleotide binding domains, NBD1 and NBD2, on each subunit it can also be classified as class I; thus, a hexameric ring contains 12 potential active sites. It was shown previously by biochemical characterizations that ClpB and Hsp104 show cooperativity between the ATPase sites (*9*, *10*) and that the subunits are tightly coupled with respect to ATPase activity, leading to impairment of activity when nonfunctional subunits are incorporated (*11*, *12*).

Because of the inherent complexity of this class I AAA+ protein, however, it has been a challenge to characterize the contribution of individual nucleotide binding domains to the overall properties of the enzyme. It has been shown for ClpB that the N-terminal domain is not needed for chaperone activity (*13*, *14*). Moreover, ClpB from *Thermus thermophilus* ($ClpB_{Th}$) can be separated into two constructs comprising amino acids 141−519 and 520−854, respectively. Individually, these constructs are still folded but do not assemble into higher oligomers such as hexamers. When the two separately purified constructs are mixed together, they form a multimeric complex and even recover chaperone activity (*15*).

In this work, we characterized the nucleotide binding properties of the construct NBD2-C (residues 520−854), which contains the second nucleotide binding domain (NBD2) and the C-terminal domain (see Figure 1). This construct provides a minimal model system for nucleotide binding to a AAA+ domain, as it contains only a single nucleotide binding domain that still binds nucleotides in isolation and even exhibits ATPase activity. In addition, it does not form higher-order oligomers such as hexamers but is rather in a monomer−dimer equilibrium

[†]The project was funded by the Max Planck Society and a Ph.D. scholarship to N.D.W. from the German National Academic Foundation.

*To whom correspondence should be addressed: Max Planck Institute for Medical Research, Department of Biomolecular Mechanisms, Jahnstrasse 29, D-69120 Heidelberg, Germany. Telephone: ++49 (6221) 486 502. Fax: ++49 (6221) 486 585. E-mail: jochen.reinstein@mpimf-heidelberg.mpg.de.

[1]Abbreviations: AAA+, ATPases associated with various cellular activities; ClpB, caseinolytic peptidase B; NBD1, nucleotide binding domain 1; NBD2, nucleotide binding domain 2; Hsp104, heat shock protein 104; $ClpB_{Th}$, caseinolytic peptidase B homologue from *Thermus thermophilus*; MANT-dADP, 2′-deoxy-3′-*O*-(*N*′-methylanthraniloyl)adenosine 5′-*O*-diphosphate; MANT-ADP, 2′(3′)-*O*-(*N*′-methylanthraniloyl)adenosine 5′-*O*-diphosphate; MANT-dATP, 2′-deoxy-3′-*O*-(*N*′-methylanthraniloyl)adenosine 5′-*O*-triphosphate; NBD2-C, construct containing NBD2 of $ClpB_{Th}$ and the C-terminal domain comprising amino acids 520−854; NBD2-C_{Trp}, tryptophan variant of NBD2-C; NBD1-M, construct containing NBD1 of $ClpB_{Th}$ and the M domain comprising amino acids 141−519; nt, nucleotide; PDB, Protein Data Bank.

 Published on Web 06/30/2009

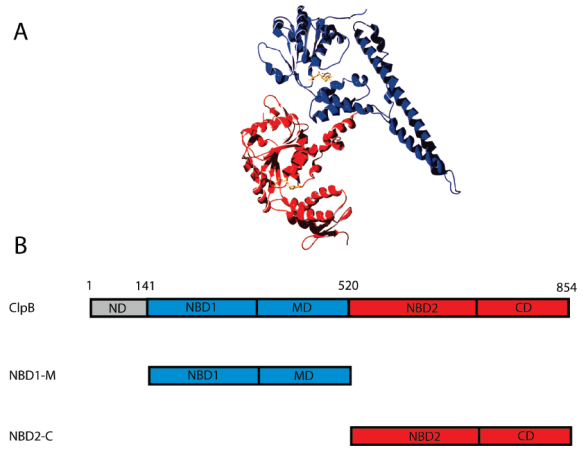

FIGURE 1: ClpB domain organization. (A) Structure of ClpB from amino acid 141 to 854 showing the two constructs NBD1-M (blue) and NBD2-C (red). Bound nucleotides are colored orange. Structural data were taken from PDB entry 1QVR (*32*), visualized by Swiss-PDB-viewer and rendered by POV-ray. (B) Domain architecture of full-length ClpB and the two constructs NBD1-M and NBD2-C.

at higher protein concentrations, which simplifies the system even more. Using this model system, we determined binding and dissociation rate constants of fluorescently labeled and unlabeled nucleotides. The information obtained was used to design more complex experiments by mixing NBD2-C with NBD1 containing construct NBD1-M (residues 141−519) and thus initiate the assembly of higher-order oligomers. We observed that NBD2 binding of the fluorescent nucleotide analogue MANT-dADP is modulated by oligomer formation, suggesting allosteric cross talk between different domains of the ClpB complex. Our results show how oligomerization can influence nucleotide binding dynamics and present a way of assigning these properties to individual domains in a complex multimeric enzyme.

EXPERIMENTAL PROCEDURES

Chemicals. Chemicals were purchased from Sigma, Merck, and Roth. MANT-ADP was synthesized as described previously (*16*). MANT-dADP and MANT-dATP were purchased from BIOLOG (Bremen, Germany).

Site-Directed Mutagenesis. NBD2-C_{Trp} is a construct of NBD2-C in which the intrinsic tryptophan residues at positions 533 and 723 were mutated to tyrosine. The tyrosine at position 799 was mutated to tryptophan. These mutations were introduced according to the Quikchange protocol (Stratagene).

Protein Expression and Purification. Protein expression and purification of NBD2-C (residues 520−854), the NBD2-C tryptophan variant, and NBD1-M (residues 141−519) were performed essentially as described previously (*15*). Proteins were expressed in Bl21(DE3) RIL cells (Stratagene) in LB medium at 37 °C and induced with isopropyl 1-thio-β-galactopyranoside (1 mM). NBD2-C was first purified by Ni-NTA chromatography and dialyzed into 50 mM Tris-HCl (pH 7.5), 300 mM KCl, 10 mM imidazole, and 10% glycerol; alkaline phosphatase (Roche) (3 units/mg of protein) was added to remove nucleotides, and the solution was incubated for 2 h at room temperature. An additional Ni-NTA purification was performed to remove alkaline phosphatase before dialysis of the pooled fractions and thrombin cleavage. The His tag, undigested protein, and thrombin were removed with a benzamidine column (Amersham) and subsequent Ni-NTA column. Remaining impurities were removed by size exclusion chromatography on a Superdex 200 column (Amersham) in 50 mM Tris-HCl (pH 7.5), 50 mM KCl, 5 mM $MgCl_2$, 2 mM EDTA, and 10% glycerol. NBD1-M was purified by the same strategy, but without alkaline phosphatase treatment because of the low affinity of isolated NBD1-M for nucleotides. Full-length $ClpB_{Th}$ was purified as described previously (*12*).

Kinetic Measurements. Stopped-flow measurements were performed with a Biologic SFM-400 instrument (BioLogic Science Instruments, Claix, France). In experiments using MANT-labeled nucleotides, excitation was at 296 nm and emission was monitored using a 400 nm long pass filter (400FG03-25, LOT Oriel Group). Experiments with the tryptophan mutant NBD2-C-799W were performed using a 320 nm long pass filter (320-FG01-25, LOT Oriel Group). Typically, two to four traces were recorded and averaged.

Binding and dissociation experiments with NBD2-C alone were performed in 50 mM Tris (pH 7.5), 200 mM KCl, 5 mM $MgCl_2$, and 2 mM EDTA and thermostated to an average temperature of 25.2 ± 0.3 °C. To strengthen the effects of complex formation, experiments that involved NBD1-M and NBD2-C were performed at lower KCl concentrations (50 mM).

Studies of temperature dependence were performed in 50 mM MOPS (pH 7.5), 200 mM KCl, 5 mM $MgCl_2$, and 2 mM EDTA.

Eyring plots were generated according to the following equation (compare to ref *17*)

$$\ln\left(\frac{kh}{k_B T}\right) = -\frac{\Delta H^{\ddagger}}{R}\frac{1}{T} + \frac{\Delta S^{\ddagger}}{R} \quad (1)$$

where k is the association or dissociation rate constant determined for the specific binding reaction, h is Planck's constant, k_B is Boltzmann's constant, R is the gas constant, and T is the absolute temperature. $\Delta H^{\ddagger}$ was determined from a plot of the term on the left side versus the reciprocal temperature ($1/T$). $\Delta G^{\ddagger}$ was determined by

$$\Delta G^{\ddagger} = -RT \ln\left(\frac{kh}{k_B T}\right) \quad (2)$$

$\Delta S^{\ddagger}$ was not determined from the Y-intercept as this is associated with a higher degree of uncertainty but from the following relationship

$$\Delta S^{\ddagger} = \frac{\Delta H^{\ddagger} - \Delta G^{\ddagger}}{T} \quad (3)$$

In sequential jump experiments, two solutions (e.g., 4 μM NBD2-C and 10 μM MANT-dADP) were mixed in a 1:1 ratio and allowed to react for a given time (delay time) in an incubation loop. In the next mixing step, the solution (e.g., 2 μM NBD2-C and 5 μM MANT-dADP) was pushed out of the incubation loop and mixed in a 1:1 ratio with 500 μM unlabeled ADP (compare Figure 2E).

For ATP/MANT-dADP competition experiments, pyruvate kinase (0.00625 mg/mL) (Roche) and 200 μM phosphoenolpyruvate (Roche) were added to ATP as well as protein solutions to remove residual ADP impurities.

Data Analysis. Transients were fitted to exponential functions using GraphPad Prism 4.0. Global analysis of sequential jump experiments of the MANT-ADP binding data was performed using Prism 4.0 (GraphPad Software, San Diego, CA) using shared rate constants among fitted transients, whereas all other parameters were allowed to vary. Numerical data analysis was performed using Dynafit (BioKin Ltd., Watertown, MA).

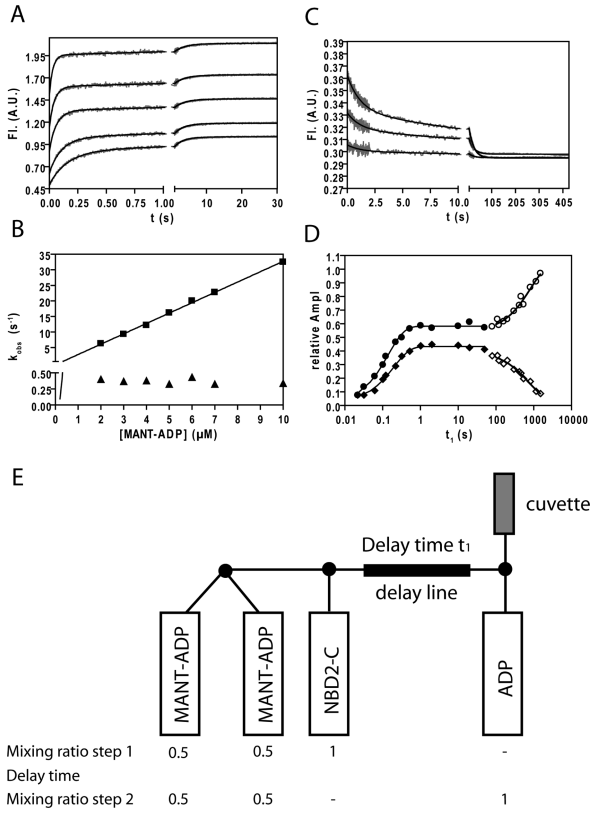

FIGURE 2: MANT-ADP binding to NDB2. (A) Rapid mixing of various MANT-ADP concentrations with NBD2-C. Gray curves (from bottom to top) represent binding traces of 1 μM NBD2-C with 2, 3, 5, 7, and 10 μM MANT-ADP (final concentrations). Solid black lines represent least-squares fits with the sum of two exponential functions. (B) Replot of observed rate constants fitted from data shown in panel A. (C) Data from sequential mixing experiments. In a first mixing step, 4 μM NBD2-C were mixed with 0.5 μM MANT-ADP in a 1:1 ratio and the solution was incubated for various delay times (t_1) and then mixed in a 1:1 ratio with 500 μM ADP. The gray traces are examples for three different delay times (from bottom to top) of 22 ms, 102 ms, and 50 s. Solid black lines are global fits to two observed rate constants, 0.87 and 0.05 s^{-1}. (D) Replot of amplitudes from data presented in panel C. Amplitudes associated with a rate constant of 0.87 s^{-1} are plotted as diamonds, and amplitudes associated with a rate constant of 0.05 s^{-1} are plotted as circles. Empty symbols depict data from manual mixing experiments. With increasing delay times, amplitudes of both exchange rates increase according to the binding rate of MANT-ADP in the first mixing step. Then the amplitude of the faster exchange rate decreases. (E) Schematic representation of the sequential mixing experiment shown in panels C and D.

The data presented in Figures 4 and 6 were fitted in a semiglobal way to the mechanism presented in Figure 3B using Dynafit 4 (essentially by numerical integration of the corresponding differential equations and nonlinear least-squares minimization). In the fitting procedure, the rate constants, k'_1, k'_{-1}, k_1, and k_{-1}, were global parameters that were shared by all data sets included in the fitting procedure leading to a global χ^2 that represents the sum of all unweighted deviations fitted to calculated data. Amplitudes were represented by response coefficients, and these were considered as semiglobal parameters that were shared by all traces of one experimental series [e.g., MANT-dADP binding kinetics with different MANT-dADP concentrations and a constant NBD2-C concentration or a double-jump experiment with different delay times (t_1)]. The offsets of each data trace were considered as local parameters that were not shared between the different data traces. For double-jump experiments, the t_1 for each datatrace could be included as a fixed parameter (incubation time). All these parameters were modified by the minimization procedure until minimal deviation between the simulations obtained by numerical integration and the experimental data was achieved.

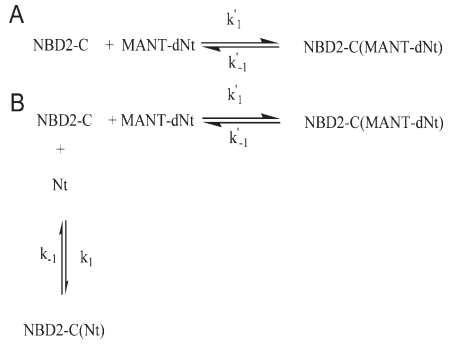

FIGURE 3: Nucleotide binding schemes. (A) Mechanism for binding of fluorescently labeled nucleotide analogues, MANT-dADP and MANT-dATP, to NBD2-C. (B) Mechanism for competition and chase experiments using labeled and unlabeled nucleotides.

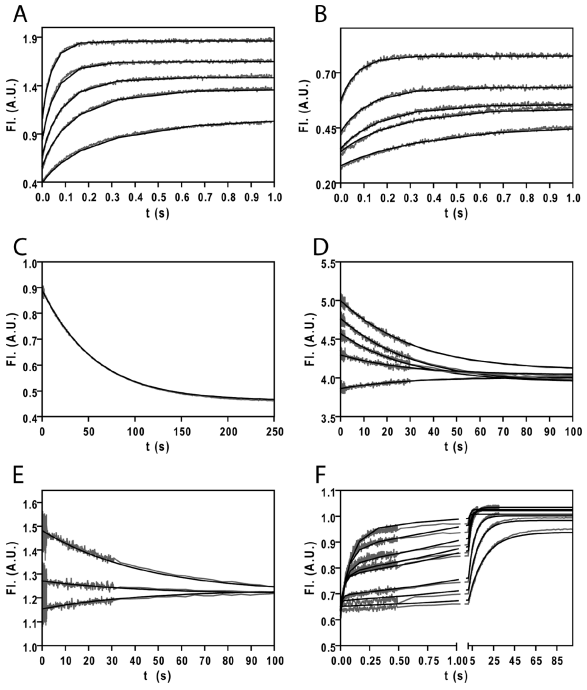

FIGURE 4: Global numerical analysis of binding of MANT-dADP and ADP to NBD2-C. Graphs A−F represent example traces of experiments taken into this global fit based on Figure 3. Binding parameters are given in Table 1. (A) NBD2-C (1 μM) was mixed with 1, 2, 3, 4.2, and 6 μM MANT-dADP (from bottom to top). (B) MANT-dADP (0.25 μM) was mixed with 0.6, 1, 1.4, 2, and 3.5 μM NBD2-C (from bottom to top). (C) MANT-dADP (5 μM) was preincubated with 2 μM NBD2-C and then mixed in a 1:1 ratio with 4 mM ADP. (D) Sequential jump experiment. MANT-dADP (10 μM) was mixed in a 1:1 ratio with 4 μM NBD2-C and incubated for a delay time (t_1) in a delay loop. After t_1, the volume in the delay loop was mixed in a 1:1 ratio with 500 μM ADP. The data represent data for different delay times: 0.032, 0.062, 0.122, 0.222, and 1.022 s (from bottom to top). (E) Sequential jump experiment in which 0.5 μM MANT-dADP was mixed in a 1:1 ratio with 4 μM NBD2-C and incubated for a delay time (t_1) in a delay loop. After t_1, the volume in the delay loop was mixed in a 1:1 ratio with 500 μM ADP. The data represent data for different delay times: 0.022, 0.082, and 0.522 s (from bottom to top). (F) NBD2-C (0.5 μM) was mixed simultaneously with 2.5 μM MANT-dADP and 0.625, 2.5, 5, 7.5, 10, 25, 50, and 100 μM ADP (from top to bottom) in a single-jump experiment. Solid black lines represent results from numerical least-squares global fits. All concentrations of single-jump experiments refer to final concentrations in the cell.

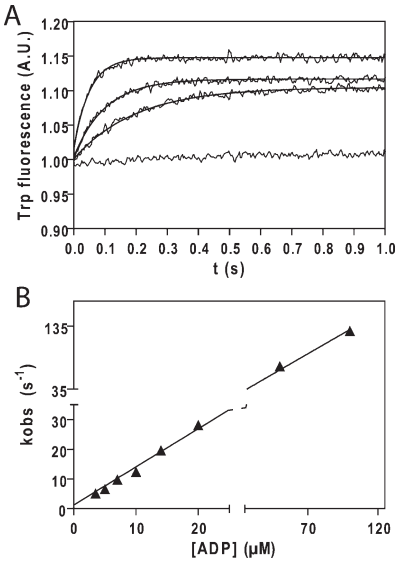

FIGURE 5: Binding of ADP to NBD2-C_{Trp}. (A) Binding of 1 μM NBD2-C_{Trp} to 3.5, 7, and 14 μM ADP (from bottom to top). The bottom line refers to mixing with buffer instead of ADP. Concentrations refer to final concentrations. Black lines represent least-squares fits to a single-exponential function. Curves are normalized to a starting fluorescence of 1. (B) Replot of the rate constants obtained from single-exponential fits. The line represents the least-squares fit with a *Y*-intercept constrained to 1.2 s^{-1} (based on the result for ADP/mant-dADP competition) and a slope of 1.3 μM^{-1} s^{-1}.

Analytical Ultracentrifugation. Sedimentation velocity runs of NBD2-C were performed with a Beckmann Proteome-Lab XL-I analytical ultracentrifuge at a speed of 40000 rpm (An-60 Ti rotor) and at 20 °C. When higher protein concentrations were used (~40 μM), sedimentation was monitored at 280 nm. Protein concentrations in the cells were then determined using initial absorption values at 280 nm and an extinction coefficient of 21430 M^{-1} cm^{-1}. At lower concentrations (3.6 μM), sedimentation was monitored at 234 nm. Data were analyzed using the time derivative analysis of the Origin-based Beckmann XL-A/XL-I data analysis software and a *c*(*s*) analysis performed with Sedfit version 9.4.c (www.analyticalultracentrifugation.com) (*18*). *c*(*s*) plots were fitted to Gaussian functions with Prism 4.0, and the area was used to estimate the amount of species in the system. The two analyses gave comparable results.

High-Performance Liquid Chromatography (*HPLC*) *Analysis*. Determination of free or protein-bound nucleotides was achieved by a TCA precipitation protocol and subsequent HPLC analysis. Sixteen microliters of the protein sample was precipitated with 4 μL of 50% TCA and incubated for 15 min on ice before centrifugation for 10 min at 13400 rpm on a tabletop centrifuge at 4 °C. Ten microliters of the supernatant was mixed with 20 μL of a 2 M potassium acetate solution before 20 μL of this mixture was applied to a C18 column (Prontosil Hypersorb ODS, 5.0 μm, l = 250 mm, d = 4.6 mm) and developed with 50 mM potassium phosphate buffer (pH 6.8). Elution was monitored by absorption at 254 nm and compared to standard runs to calculate impurities of adenine nucleotides. Calculated impurities after alkaline phosphatase treatment and purification were less than 5%.

Analysis of MANT-ADP isomers was performed on a C18 column (Prontosil Hypersorb ODS, 5.0 μm, l = 250 mm, d = 4.6 mm) in 20 mM potassium phosphate buffer (pH 6.8) using an acetonitrile gradient between buffer A [20 mM potassium phosphate buffer (pH 6.8) and 4% acetonitrile] and buffer B [20 mM potassium phosphate buffer (pH 6.8) and 14% acetonitrile]. The HPLC program was run with a linear gradient from 65 to 100% buffer B for 20 min at a flow speed of 1.5 mL/min and then for an additional 15 min at 100% buffer B. Two shoulders could be detected in the elution profile. To test the influence of NBD2-C on the distribution of MANT-ADP isomers, 150 μM NBD2-C was preincubated with 40 μM MANT-ADP for 45 min at room temperature before the protein was precipitated as described above, but using a 0.4 M potassium acetate solution instead of a 2 M solution to slow the reisomerization process with a lower pH. Samples were analyzed as described above but using MANT-specific fluorescence instead of UV absorption. To estimate the ability of NBD2-C to hydrolyze dATP and MANT-dATP, NBD2-C (150 μM) was incubated with 100 μM MANT-dATP in 50 mM Tris (pH 7.5), 50 mM KCl, 5 mM $MgCl_2$, and 2 mM EDTA. Samples were taken manually and analyzed as described above.

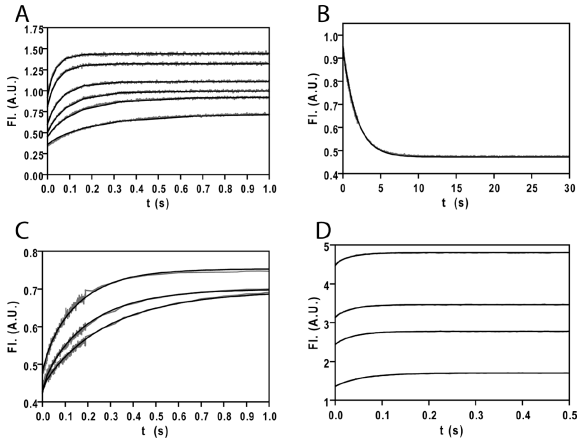

FIGURE 6: Global numerical analysis of binding of MANT-dATP and ATP to NBD2-C. (A and B) Example traces for experiments used to globally fit MANT-dATP binding data. (C and D) ATP binding data. Binding parameters for MANT-dADP and ADP included in the fit were obtained from previous analysis (Figure 3). (A) NBD2-C (1 μM) was mixed with 1, 2, 3, 4.2, 6, and 7.5 μM MANT-dATP (from bottom to top). (B) MANT-dATP (5 μM) was preincubated with 2 μM NBD2-C and then mixed in a 1:1 ratio with 250 μM ADP. (C) NBD2-C (0.5 μM) was mixed with 2.5 μM MANT-dADP and 40, 80, and 160 μM ATP (from top to bottom). ATP and protein solutions were preincubated with 0.00625 mg/mL pyruvate kinase and 200 μM PEP. (D) NBD2-C (1 μM) was preincubated with 200 μM ATP, 0.00625 mg/mL pyruvate kinase, and 200 μM PEP and then mixed in a 1:1 ratio with different amounts of MANT-dADP (from bottom to top): 25, 50, 70, and 100 μM. All concentrations are final concentrations in the cell, if not stated otherwise. Black lines represent least-squares fits of the numerical analysis. Parameters of the fits are given in Table 1.

RESULTS

Biochemical and Biophysical Properties of NBD2-C. This study used the C-terminal part of ClpB from *T. thermophilus*, comprising amino acids 520−854, which constitute a AAA+ nucleotide binding domain and a C-terminal extension (NBD2-C). NBD2-C is able to form homodimers in a salt-dependent fashion, as could be shown by gel filtration experiments (*15*). These homodimers are considered to be the ATPase active units (*15*). To study the dimerization of NBD2-C in more detail, we used analytical ultracentrifugation sedimentation velocity experiments at monomer concentrations between 29 and 34 μM and at different salt concentrations. In buffer containing 50 mM Tris (pH 7.5), 200 mM KCl, 5 mM $MgCl_2$,

and 2 mM EDTA, the ratio of monomers to dimers was approximately 1:1. The fact that the two peaks had no baseline separation in $c(s)$ distributions suggests that the two forms are in rapid equilibrium on the time scale of the ultracentrifugation experiment. As also observed for the oligomeric states of the ClpB holoenzyme (*10*, *19*), the oligomerization of NBD2-C was salt-dependent. At 50 mM KCl, the ratio of NBD2-C monomers to NBD2-C dimers was 1:3, and at 500 mM KCl, it was 1:0.8, confirming previous gel filtration results showing that lower salt concentrations favor dimer formation (*15*). Furthermore, the data suggest that the K_D between two NBD2-C molecules is in the higher micromolar range, since otherwise almost exclusively dimers would be observed at the high concentrations used in the ultracentrifugation experiment. At the lower concentrations of NBD2-C used in other biochemical and biophysical experiments (0.5−10 μM), we would therefore expect the equilibrium to lie even more in favor of the monomeric species. We then performed another ultracentrifugation experiment under low-salt conditions (50 mM KCl) using 3.6 μM NBD2-C monomer, where one might expect dimers, but only one species (equivalent to a monomer) was observed; this suggests that the monomer is the predominant species at concentrations in the lower micromolar range.

Binding of Adenosine Diphosphates to NBD2-C. To investigate the nucleotide binding properties of NBD2-C, we used fluorescent nucleotide analogues. Previous studies on NBD2-C reported a tight binding of MANT-ADP with a K_D of 0.07 μM (*15*). Here the fluorophore (*N*′-methylanthraniloyl) is attached to the 2′- or 3′-hydroxyl group of the ribose. MANT-labeled nucleotides always consist of a mixture of isomers comprising approximately two-thirds of the 3′ form and one-third of the 2′ form, and the isomerization is pH-dependent. For MANT-GTP, the isomerization process has a half-life of ~7 min at pH 7.4 and 20 °C (*20*). Thus, when using MANT analogues in kinetic studies, the data should be treated with care as isomerization phases and the different binding properties of the two isomers might cause phases that are not related to the biologically relevant binding process (*21*, *22*). Nevertheless, in many cases, binding of MANT-ADP or MANT-ATP has provided important insights into the nucleotide binding properties of enzymes (*23*−*27*). We therefore started a series of stopped-flow experiments using MANT-ADP and NBD2. Mixing of 1 μM NBD2-C with excess amounts of nucleotides resulted in stopped-flow traces that could be fitted with two exponential phases in the first 30 s (Figure 2). The rate constants of the faster phase increased linearly with nucleotide concentration with a slope of 3.3 μM^{-1} s^{-1}, indicative of initial complex formation, whereas the slower phase was nucleotide-independent with an apparent rate constant of ~0.3 s^{-1}. This phase was not observed in experiments in which NBD2-C was in excess over MANT-ADP. We show below that this slower phase is likely to arise from small contaminations of residual nucleotide bound to the purified protein (despite alkaline phosphatase treatment during the purification procedure). This phase will be neglected in our interpretation of the data. At longer recording times, an additional slow phase appeared with an apparent rate constant of 0.02 s^{-1}, which could suggest a process associated with isomerization of MANT-ADP (*21*). A similar slow phase (of ~0.01 s^{-1}) was observed when prebound MANT-ADP was chased by excess amounts of unlabeled ADP. These slow isomerization phases can be rationalized as follows. NBD2 binds one of the isomers preferentially, causing a perturbation of the equilibrium mixture of the two forms which then leads to (slow) reisomerization. To test this hypothesis further and to estimate the differences in binding of the two isomeric forms, we performed an additional experiment based on two sequential mixing steps. In a first step, MANT-ADP was mixed with excess of NBD2 and incubated for various delay times (t_1) between 22 ms and 100 s; then, in a second mixing step, the solution was mixed with excess amounts of unlabeled ADP. Two exponential phases representing nucleotide exchange were observed (0.87 and 0.05 s^{-1}), and amplitudes of both phases increase with t_1, suggesting that the two MANT-ADP isomers bind with similar rates to NBD2 but dissociate at rates differing by 1 order of magnitude (Figure 2D). To obtain data for t_1 values of > 100 s, we mixed MANT-ADP and protein manually and performed the second mixing step in a regular stopped-flow setup. At longer t_1 times, the amplitude of the faster exchange rate decreased to almost zero with an apparent rate constant of 0.001 s^{-1}, whereas the amplitude associated with the slower exchange rate increased with a similar rate constant, suggesting that NBD2 indeed shifts the equilibrium of the two isomers by binding one of them preferentially (Figure 2D). HPLC analysis in the presence and absence of NBD2-C confirmed this finding and suggests, on the basis of the relative fluorescence intensities of the two forms (*21*), that 3′-MANT-ADP is the isomer that binds to NBD2 with higher affinity (data not shown). In summary, we find that MANT-ADP binds tightly to NBD2-C, but the two MANT-ADP isomers bind to the protein with different affinities, which can cause artificial phases and make a detailed analysis of the complex binding kinetics more difficult. The fact that the binding properties of the two MANT isomers differ so significantly suggests that kinetic studies of other AAA+ proteins using these nucleotides should be interpreted very carefully, not just with respect to small isomerization phases.

For further nucleotide binding studies, we used the fluorescent nucleotide analogue MANT-deoxy-ADP (2′-deoxy-3′-MANT-ADP), which lacks the 2′-hydroxyl group and therefore cannot isomerize. Binding of 1 μM NBD2 to excess MANT-dADP could be described by two exponential functions. In agreement with our previous interpretation of the data, the very slow phase measured for MANT-ADP binding was not observed here. The rate constants of the fast phase again increased linearly with MANT-dADP concentration with a slope of 4.6 μM^{-1} s^{-1}, and the slower phase (~0.25 s^{-1}) was rather independent of the nucleotide concentration. As observed for MANT-ADP, this slower phase disappeared when the protein was in excess over nucleotide, which could be interpreted as heterogeneity in the ensemble of NBD2-C. Several reasons could account for the observed heterogeneity. Not only the existence of two isomeric states of NBD2 that bind nucleotide differently but also dimerization, minor fractions of phosphate-, pyrophosphate-, or sulfate-binding species or remaining fractions of NBD2-C-bound ADP even after the purification procedure could explain such a nucleotide-independent phase. Several of these possibilities were tested by measuring the dependence of rates and relative amplitudes on NBD2-C concentration, by addition of phosphate, sulfate, or pyrophosphatase in the assay, and these showed no influence. However, the phase was affected by preincubation with pyruvate kinase (which does not react with MANT-dADP) and phosphoenolpyruvate in the stopped-flow solutions, resulting in a reduction of more than 50% of the amplitude, whereas the fast, nucleotide-dependent phase remained unaffected. This result suggests that the slow phase observed upon rapid mixing with

Table 1: Binding Parameters As Calculated from Global Analysis[a]

		NBD2-C_{wt}	NBD2-C_{Trp}
MANT-dADP	k'_1 (μM^{-1} s^{-1})	4.2 (± 0.02)	3.4 (± 0.012)
	k'_{-1} (s^{-1})	0.015 (± 6×10^{-5})	0.016 (± 1×10^{-4})
	$K'_{D(calc)}$ (μM)	0.004 (± 2×10^{-5})	0.005 (± 3×10^{-5})
MANT-dATP	k'_1 (μM^{-1} s^{-1})	3.9 (± 0.01)	nd[b]
	k'_{-1} (s^{-1})	0.53 (± 2×10^{-3})	nd[b]
	$K'_{D(calc)}$ (μM)	0.14 (± 6×10^{-4})	nd[b]
ADP	k_1 (μM^{-1} s^{-1})	2.3 (± 0.04)	1.4 (± 0.02[c]) 1.3 (± 0.03[d])
	k_{-1} (s^{-1})	1.2 (± 0.02)	1.2 (± 0.01[c]) 1.2 (± 0.005[d])
	$K_{D(calc)}$ (μM)	0.5 (± 0.01)	0.8 (± 0.01[c]) 0.9 (± 0.02[d])
ATP	k_1 (μM^{-1} s^{-1})	0.4 (± 0.01)	nd[b]
	k_{-1} (s^{-1})	35 (± 0.5)	nd[b]
	$K_{D(calc)}$ (μM)	88 (± 3)	nd[b]

[a] Parameters obtained for different nucleotides obtained from global fits of various data sets. Errors represent standard errors of the fits. NBC2-C wild-type parameters presented here were obtained from numerical fitting; however, analytical approaches (where performed) led to similar results. NBD2-C_{Trp} measurements were performed to confirm the results with a direct spectroscopic probe, i.e., direct tryptophan fluorescence, for ADP binding. [b] Not determined. [c] Results from a global fit using MANT-dADP/ADP competition experiments and numerical analysis. [d] Results from analytical analysis as described in the text.

excess amounts of MANT-dADP arises from a small nucleotide contamination even after alkaline phosphatase treatment during the purification procedure. We therefore exclude this slower process from our interpretation, and in the analysis described below, the data were truncated at longer times. The simplest model for explaining the data for binding of MANT-dADP to NBD2 was therefore reduced to a one-step mechanism for binding to monomeric NBD2-C (Figure 3).

In the next step, we set up a global fit with data from different stopped-flow experiments: (1) MANT-dADP in excess over protein, (2) protein in excess over MANT-dADP, (3) sequential mixing experiments with MANT-dADP binding in a first mixing step and then, after various delay times (t_1), mixing with an excess of unlabeled ADP, and (4) simultaneous mixing with labeled (MANT-dADP) and unlabeled (ADP) nucleotides. This set of data contains information not only about the binding of labeled nucleotide but also, in particular, data set 4, about the unlabeled nucleotide, ADP (*28*). The simulated curves describe the data well, as can be seen in Figure 4. The microscopic rate constants obtained are presented in Table 1. The rate constants k'_1 and k'_{-1} that represent the binding and dissociation rate constants of NBD2-C and MANT-dADP were found to be to 4.2 μM^{-1} s^{-1} and 0.015 s^{-1}, respectively, which results in a K'_d of 0.004 μM for the binding of MANT-dADP. For unlabeled ADP, k_1 and k_{-1} equaled 2.3 μM^{-1} s^{-1} and 1.2 s^{-1}, respectively, which gives a K_d of 0.5 μM.

By globally numerically fitting the data, we could not only integrate different experimental data and approaches into one model but also include data that are not amenable to pseudo-first-order analysis. However, the results of the global numerical fitting were in good agreement with results obtained from pseudo-first-order analysis, suggesting that both approaches lead to the same results.

To substantiate the ADP binding data obtained by kinetic competition experiments, we designed a variant of NBD2-C that changes its intrinsic tryptophan fluorescence upon binding of unlabeled nucleotide (NBD2-C_{Trp}). We replaced the two intrinsic tryptophans at positions 533 and 723 with tyrosines and introduced a tryptophan at position Y799, a position that exhibited nucleotide-sensitive fluorescence changes in the ClpB homologue Hsp104 (*29*). ADP binding resulted in a monoexponential fluorescence increase (see Figure 5), and the observed rate constants increased linearly with the concentration of ADP with a slope of 1.3 μM^{-1} s^{-1}. No slow, nucleotide-independent phase could be observed, which agrees with our previous findings and interpretations of the MANT-dADP data. The dissociation rate constant of 1.2 s^{-1} was determined by chasing 1 μM preincubated NBD2-C_{Trp} (ADP) with excess amounts of MANT-dADP (25 μM). Next, we tested whether the two methods, the direct measurement of tryptophan fluorescence and the indirect measurements using MANT-dADP/ADP mixing experiments, result in the same parameters for the association and dissociation rate constants of unlabeled ADP. Therefore, we also assessed MANT-dADP and MANT-dADP/ADP binding for the tryptophan mutant. Parameters of binding and dissociation of MANT-dADP according to Figure 3 are as follows: k'_1(MANT-dADP) = 3.4 μM s^{-1}, and k'_{-1}(MANT-dADP) = 0.016 s^{-1}. For binding and dissociation of unlabeled ADP, the fitted parameters are 1.4 μM s^{-1} and 1.2 s^{-1}, respectively, which are in excellent agreement with the results obtained from the analysis of the tryptophan fluorescence data (see Table 1). This test confirms that, even without having a probe to monitor unlabeled nucleotides directly, indirect measurements using MANT-dADP/nt competition experiments provide enough information to extract binding parameters of unlabeled nucleotides reliably.

Binding of Adenosine Triphosphates to NBD2-C. Steady state ATPase data and equilibrium titrations suggest that compared to ADP, ATP is bound to NDB2 with a much lower affinity (*10*, *15*, *29*). The steady state parameters for NBD2-C were established by Beinker et al. (*15*), with a k_{cat} of 0.115 s^{-1} and a K_M of 760 μM (at 25 °C and 10 μM NBD2-C), whereas we showed above that ADP binds with a K_D of 0.5 μM. This situation can cause misleading results as very small contaminations of ATP solutions (e.g., 1% ADP) can give rise to complex kinetics due to ADP/ATP competition. To avoid this, we preincubated the protein solution as well as the ATP solution with phosphoenolpyruvate and enzymatic amounts of pyruvate kinase and therefore eliminated most of the residual ADP in our assay solutions. When we then performed simultaneous mixing of ATP and MANT-dADP with NBD2-C, only one phase could be observed, which slowed with increasing amounts of ATP (Figure 5). This is the expected behavior for a weak binding ligand that is characterized by a high dissociation rate constant (*28*). Unfortunately, we cannot extract rate constants for ATP binding and dissociation from these data. To further constrain the parameters, we performed another experiment. We preincubated 200 μM ATP with 1 μM NBD2-C in the presence of pyruvate kinase and phosphoenolpyruvate and then mixed this solution with different MANT-dADP concentrations [final concentrations of 12.5−100 μM (Figure 6)]. Numerical global fitting of these data (together with the previous competition experiment) resulted in a K_D of 88 μM with a k_1 of 0.4 μM^{-1} s^{-1} and a k_{-1} of 35 s^{-1} for ATP binding. We tried to confirm these results by a direct change in tryptophan fluorescence upon binding of ATP to NBD2-C_{Trp}. However, no change in fluorescence could be observed even at 1000 μM ATP.

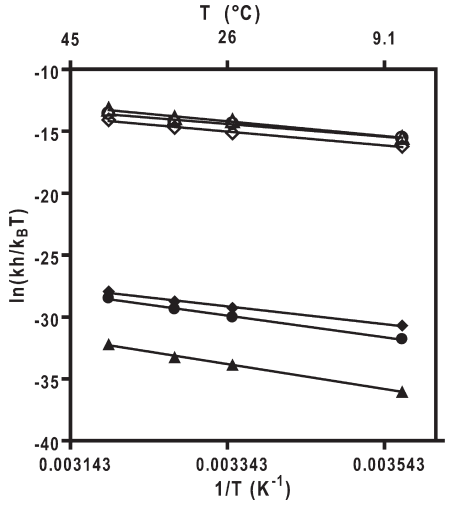

FIGURE 7: Temperature dependence of association and dissociation rate constants. Empty symbols represent data for association reactions and filled symbols data for dissociation reactions of MANT-dATP (circles), MANT-dADP (triangles), and ADP (diamonds). Thermodynamic parameters derived from these data are presented in Table 2.

To investigate the kinetic effects of the additional phosphate group in more detail, we measured the binding kinetics of MANT-dATP. The binding traces resembled those of MANT-dADP described before, so the same kinetic model was used in the analysis of the data. The fitted association rate constant (k'_1) was 3.9 μM^{-1} s^{-1}, not significantly different from the MANT-dADP association rate constant, yet the dissociation rate constant was higher by a factor of ~40 [k'_{-1}(MANT-dATP) = 0.53 s^{-1}] (Figure 6 and Table 1). This result is in good agreement with binding of unlabeled ADP and ATP, where dissociation rate constants differed by a factor of approximately 30 (Table 1), and suggests that to some extent MANT-dATP can serve as a model compound for describing the effect of the γ-phosphate on nucleotide binding of NBD2. Furthermore, HPLC analyses suggest that dATP can be hydrolyzed by NBD2-C under single-turnover conditions (> 2 min^{-1} at room temperature) and even MANT-dATP can be hydrolyzed, although much more slowly (~0.3 min^{-1}), suggesting that dATP and MANT-dATP are substrates of the NDB2 ATPase domain.

Temperature Dependence of Nucleotide Binding. NBD2-C is a construct of ClpB from the thermophilic bacterium *T. thermophilus*, a eubacterium thriving at temperatures between 50 and 80 °C. To study energetic aspects of nucleotide binding but also to investigate the effect of higher temperatures on the nucleotide binding properties, we performed binding and dissociation experiments at different temperatures. The established one-step binding mechanism at 25 °C appeared to be unaffected at temperatures ranging from 7.4 to 55 °C. Furthermore, the temperature dependence appeared to be linear without any break that would suggest a change in mechanism or rate-limiting steps with a change in temperature (Figure 7). An Eyring plot analysis suggests that for ADP, MANT-dADP, and MANT-dATP, the enthalpy term, derived from the slope of the Eyring plot, has the greatest influence on the transition state energetics of association as well as dissociation of nucleotide (Figure 7 and Table 2). This is reflected in the significant temperature dependence of k_1 and k_{-1}. The entropy term ($T\Delta S$) for the overall binding reaction was positive, indicating a gain of entropy upon binding. The entropy term of a binding reaction integrates contributions of different molecular processes: (i) change in degrees of freedom of the bound ligand, (ii) change in degrees of freedom of the amino acids that directly or indirectly participate in the binding reaction, and (iii) solvent effects. As processes (i) and (ii) are likely to reduce the entropy in a binding reaction, we surmise that the entropic effects mainly originate from release of water molecules bound to the binding interface of the protein (*30*, *31*).

Table 2: Transition State Energies for Binding (k_{on}) and Dissociation (k_{off}) of Nucleotides and Energies for the Overall Binding Reaction [$K_{D(calc)}$][a]

		ΔG (kJ/mol)	ΔH (kJ/mol)	$-T\Delta S$ (kJ/mol)
MANT-dADP	k_{on}	35 ± 0.01	49 ± 4	−14 ± 4
	k_{off}	84 ± 0.02	84 ± 3	0 ± 3
	$K_{D(calc)}$	−49 ± 0.02	−34 ± 5	−15 ± 5
MANT-dATP	k_{on}	36 ± 0.01	42 ± 4	−7 ± 4
	k_{off}	75 ± 0.01	73 ± 3	2 ± 4
	$K_{D(calc)}$	−39 ± 0.01	−30 ± 5	−9 ± 5
ADP	k_{on}	38 ± 0.03	47 ± 3	−9 ± 3
	k_{off}	73 ± 0.03	60 ± 4	13 ± 4
	$K_{D(calc)}$	−35 ± 0.04	−13 ± 5	−22 ± 5

[a] Energies calculated for 25.4 °C. Errors for ΔG are calculated on the basis of the standard errors of the fitted kinetic primary data. Errors for ΔH are based on the error of the linear slope of the Eyring plot, and errors for ΔS are based on error propagation from ΔH and ΔG (compare eq 3 in Experimental Procedures).

In a graphical representation (Figure 7), it becomes particularly apparent that the association rate constants for MANT-dADP, MANT-dATP, and ADP are comparable and exhibit a similar temperature dependence. Further, the Eyring plot analysis indicates that the contributions to the transition state energetics are also very similar (Table 2), suggesting that the interaction of the enzyme with the MANT group and diphosphate specific interactions are formed after the transition state of the binding reaction.

NBD2 in the Assembled Chaperone. Heterogeneity of oligomeric species and the existence of another nucleotide binding domain hamper the detailed analysis of full-length ClpB and can even render it practically impossible without prior knowledge. Beinker and co-workers showed that NBD2-C can form multimeric assemblies when it is mixed with the separately expressed N-terminal part (NBD1-M) of ClpB. This complex even regained chaperone activity, suggesting that covalent linkage of the two domains is not mandatory for the mechanism of action (*15*).

Having characterized nucleotide binding properties of NBD2-C in isolation, we asked how these properties change in full-length ClpB. Using separately expressed NBD2-C and the NBD1-containing construct NBD1-M (Figure 1), we could compare features of NBD2 in isolation and (after mixing with NBD1) NBD2 incorporated into higher-order oligomers. In a first application of this strategy, we measured the nucleotide exchange kinetics of NBD2. To facilitate formation of the complex, these measurements were performed at lower salt concentrations (50 mM KCl). NBD2-C was preincubated with MANT-dADP in a substoichiometric ratio (2 μM NBD2 and 1.5 μM MANT-dADP). Given the dissociation constant of 4 nM, almost no free MANT-dADP should be present in solution. When the sample was chased with excess amounts of unlabeled ADP, the exchange trace of NBD2-C alone under these conditions could be fitted with a monoexponential function with a rate constant of 0.011 s^{-1} (Figure 8). When we mixed this complex with the NBD1 construct and excess amounts of ADP (final

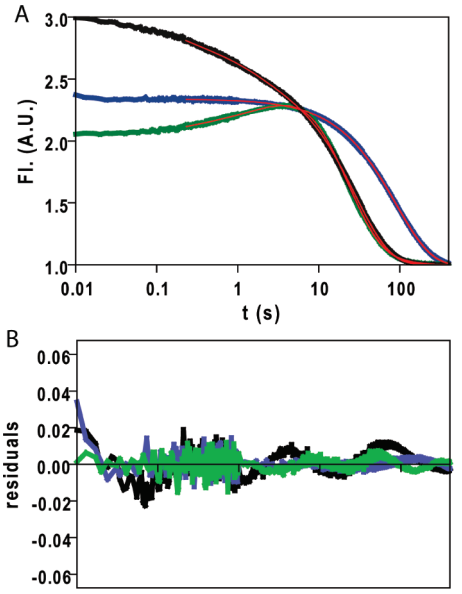

FIGURE 8: Exchange kinetics of NBD2 alone and reconstituted chaperone. (A) NBD2-C (2 μM) was preincubated with 1.5 μM MANT-dADP and mixed in a 1:1 ratio with 5 mM ADP (blue line) or 5 mM ADP and 2.5 μM NBD1-M (green line). Full-length ClpB (2 μM) was preincubated with 5 μM MANT-dADP and chased by being mixed in a 1:1 ratio with 5 mM ADP (black line). To facilitate comparison, data were normalized, so that end points of all traces are 1.0. Red lines represent least-squares fits to exponential functions as explained in Results. (B) Residuals of the least-squares fits to exponential functions (color code as in panel A).

concentration of 2.5 mM), we expected to see, after the assembly of the domains, the dissociation process of MANT-dADP from NBD2 incorporated into the assembled chaperone. As one can see in Figure 8, we did indeed see an initial increase in fluorescence, which would represent the assembly of the complex, and then a slow decrease representing exchange of MANT-dADP for unlabeled ADP. The trace was rather complex and was fitted to the sum of four exponential functions, with two phases accounting for the initial increase (3.5 and 0.28 s^{-1}). Two further exponential functions accounted for the decrease in fluorescence, one of which was fixed to the rate constant determined for NBD2-C alone (0.011 s^{-1}) to describe residual uncomplexed NBD2-C. The other rate constant (with ~95% of the amplitude of the fluorescence decrease) was fitted to 0.047 s^{-1}. Thus, nucleotide exchange was accelerated approximately 4-fold (from 0.011 to 0.047 s^{-1}), suggesting that the full-length context modulates nucleotide binding properties, specifically nucleotide exchange. Nucleotide exchange experiments with full-length ClpB supported this finding. For wild-type ClpB, three rate constants were observed when 1 μM ClpB and 2.5 μM MANT-dADP were chased with excess amounts of ADP ($k_{ex1} = 5.8\ s^{-1}$, $k_{ex2} = 0.76\ s^{-1}$, and $k_{ex3} = 0.036\ s^{-1}$), with k_{ex3} being associated with 77% of the total amplitude. This is in good agreement with the k_{ex} determined from reconstituted ClpB.

In summary, these data suggest that complex formation modulates nucleotide binding properties, in particular the nucleotide exchange rate. With our modular approach and our solid knowledge of isolated NBD2-C, we could unambiguously assign these properties to NBD2.

DISCUSSION

In this work, we followed a "bottom-up" approach to study a multimeric AAA+ enzyme with many potential nucleotide binding sites. We reduced the complexity by studying a much simpler system first, namely the second AAA+ domain, NBD2. This system still displayed many kinetic phases that we studied in detail with numerous controls, ultimately leading to a simple one-step binding mechanism. We substantiated this mechanism with a change in probe from nucleotide-linked MANT fluorescence to intrinsic tryptophan fluorescence of an engineered NBD2-C variant.

Our pre-steady state analysis of nucleotide binding to NBD2-C showed that binding of ADP and ATP requires neither oligomerization of the full-length ClpB complex nor formation of NBD2 dimers. This is understandable given the structural architecture of the construct. All common key residues involved in nucleotide binding are present on a single protomer and are cis-acting, such as hydrophobic amino acids that interact with the base, the Walker A motif which interacts with the phosphate groups, or the sensor 2 arginine (*32*), which is trans-acting in some other AAA+ proteins, such as the MCM helicases (*33*). The association rate constants for MANT-dADP (4.2 $\mu M^{-1}\ s^{-1}$), MANT-dATP (3.9 $\mu M^{-1}\ s^{-1}$), ADP (2.3 $\mu M^{-1}\ s^{-1}$), and ATP (0.4 $\mu M^{-1}\ s^{-1}$) are similar and are in good agreement with those determined for other nucleotide binding enzymes (*17*, *23*, *24*). The data suggest that specific interactions that discriminate between di- and triphosphates are formed later in the binding reaction, i.e., after the transition state. As a consequence, differences between the nucleotides are very pronounced in the dissociation rate constants. MANT-dADP dissociation is slower by almost 2 orders of magnitude than MANT-dATP and ADP (see Table 1). For ATP, a dissociation rate constant of 35 s^{-1} was determined, which differs by more than 3 orders of magnitude from that of MANT-dADP.

The presented kinetic rate constants show that ATP binding and dissociation processes are much faster than the hydrolysis rates measured for NBD2 (*15*). In this way, ClpB NBD2 ATP binding differs from that of other AAA+ domains like those in ClpX and HslU, where ATP hydrolysis seems to be much faster than ATP dissociation (*34*, *35*).

The temperature dependence of MANT-dADP, MANT-dATP, and ADP binding revealed that the binding reactions have a significant enthalpic contribution, but also a favorable entropic part, suggesting the liberation of water upon binding of nucleotides.

Our data show that binding of MANT-ADP to NBD2-C causes a shift of the 2′/3′-MANT-ADP equilibrium, due to preferential binding of the 3′-MANT-ADP form by NBD2-C. This finding implies two interesting points. In a first approximation, NBD2-C seems to have strong favorable interactions with the 3′-MANT group, which are partly responsible for the difference in the affinity of the 2′ and 3′ isomers and are likely to contribute to the strong binding to 3′-MANT-2′-dADP. An inspection of 3′-MANT-ADP modeled into the X-ray structure of NBD2 (unpublished results) indicated that the *N*′-methylanthraniloyl group occupies free space and does not clash with the nucleotide binding pocket, similar to the situation for NBD1 (*36*), whereas 2′-MANT-ADP is sterically less favored. Furthermore, there are a number of amino acids in the vicinity of the nucleotide that could interact with the 3′-label. Possible interactions are a hydrogen bond between Glu603 and the carbonyl of the MANT-dADP ester group and a cation-π interaction between Lys606 Nη and the benzene ring. The polar nature of these possible interactions agrees with the temperature dependence of the NBD2−MANT-dADP binding affinity. For hydrophobic interactions, we would expect to see an increase in affinity with higher

temperatures, whereas our data revealed a slight decrease in MANT-dADP affinity.

Second, we show that MANT isomerization can cause artificial phases which can easily be misinterpreted. This becomes particularly important when more complex systems are studied, such as the full ClpB complex with potential asymmetric nucleotide binding sites. Effects of the heterogeneity of the nucleotide could then be mistakenly interpreted as heterogeneity or asymmetry of the protein complex studied.

Our data for the fluorescent nucleotides as well as for unlabeled nucleotides show that binding of the diphosphate has a much higher affinity than binding of the triphosphate (by approximately 2 orders of magnitude), which is in agreement with previous equilibrium studies of full-length ClpB (*10*) and Hsp104 (*29*). However, the strong preference for ADP with a K_D which is smaller by 200-fold is extremely pronounced in this case. This situation leads to a number of unusual observations. Residual concentrations of ADP can lead to slow phases in the binding of fluorescent nucleotide analogues, as well as in the binding of unlabeled ATP. The high affinity for ADP can also account for the discrepancy between the K_D for ATP and the K_M measured for NDB2-C in steady state ATPase assays (*15*). In a system where the K_D for ADP is extremely low, even marginal steady state concentrations of ADP are sufficient to increase the apparent K_D by several-fold, according to the equation for competitive inhibition (*37*)

$$v = \frac{[E]_0[ATP]k_{cat}}{[ATP]+K_M[1+\frac{[ADP]}{K_{D(ADP)}}]}$$

Here a steady state ADP concentration of 2 μM [with a $K_{D(ADP)}$ of 0.5 μM] would increase the apparent K_M by a factor of 5, but when we compare our binding data with the steady state ATPase data, there is yet another interesting feature that needs to be discussed. The sigmoidal shape of the curve of ATPase activity can be described by a Hill coefficient of 2.1 (*15*). A model that is based on a NBD2-C dimer as the functional ATPase and on the assumption that ATPase activity is greatly increased when both ATP binding sites on the dimer are occupied can account for this feature. Then the second (and visible) macroscopic dissociation constant is higher than the microscopic K_D for ATP, and the system exhibits a sigmoidal response. Another explanation for the discrepancy between K_D and K_M could be that dimerization of NBD2-C is coupled to formation of asymmetric ATP binding sites on the NBD2-C dimer. Asymmetric ATP binding sites are not unusual among AAA+ proteins (*35*, *38*, *39*), and it could be shown for the Lon protease that the lower-affinity ATP binding sites represent the ATPase active sites (*38*, *40*). For NBD2-C, this explanation is possible but has not been supported by other experimental evidence thus far.

Considering the function of ClpB in disaggregating protein aggregates and the proposed mechanisms and crystal structures for other AAA+ proteins, it is very surprising that no conformational change can be detected upon binding of ADP and ATP. Our measurements could always be described sufficiently by a simple binding model according to Figure 3, and there was no clear indication of a conformational change, even at higher temperatures. It is possible that significant conformational changes occur only in the functional dimeric complex of NBD2-C or that conformational changes are not detectable because they are fast and not rate-limiting. One of the key concepts of catalysis is the stabilization of the transition state and destabilization of the ground state to accelerate reactions. In this way, conformational changes could also lead to high-energy intermediates that are not populated in binding experiments but only in a reaction cycle that imposes directionality on the process.

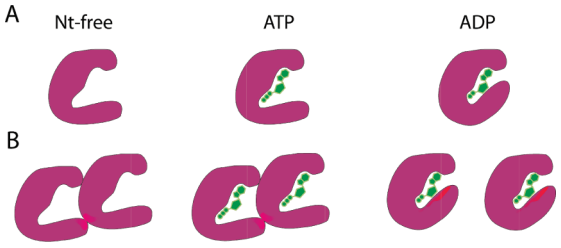

FIGURE 9: Hypothetical model visualizing properties of different NBD2-C conformations. (A) The nucleotide-free and ATP-bound conformations are similar. As a consequence, NBD2-C_{Trp} does not undergo a change in tryptophan fluorescence upon binding of ATP. The conformation is open, in agreement with the high dissociation rate constant of bound ATP. The ADP conformation is different from the nt-free and ATP-bound conformation; consequently, NBD2-C_{Trp} increases fluorescence upon binding. Further, the dissociation rate constant of ADP is lower by a factor of 30, suggesting a closed conformation. (B) The properties described in panel A are in good agreement with the oligomerization properties of full-length $ClpB_{Th}$. nt-free and ATP-bound $ClpB_{Th}$ form higher-order oligomers, whereas ADP-bound $ClpB_{Th}$ dissociates into lower-order oligomers.

However, a closer look at the data suggests significant changes between the conformations of ADP- and ATP-bound NBD2-C. First, ADP binding increases the tryptophan fluorescence of the NBD2-C variant NBD2-C_{Trp}, whereas ATP binding does not cause a significant change in fluorescence. This suggests that ADP binds to a structure that is different from the nucleotide-free state and that ATP binds to a conformation that is similar to the nucleotide-free state, at least as probed by the environment of the tryptophan. Furthermore, the difference in the dissociation rate constants between di- and triphosphates suggests a closed conformation for ADP-bound NBD2-C and an open conformation for ATP-bound NBD2-C (Figure 9A) with a dissociation rate which is 30-fold higher than that for ADP. These observations for NDB2-C are in agreement with previous results on the oligomerization properties of $ClpB_{Th}$. In the presence of ATP or in the absence of nucleotides, $ClpB_{Th}$ forms higher-order oligomers, whereas lower-order oligomers are populated in the presence of ADP (*41*). These effects are not pronounced when nucleotide binding to the second NBD is impaired (*12*), suggesting that indeed nucleotide-dependent conformational changes in NBD2 trigger dissociation and that the ATP and nucleotide-free form are to some extent similar but different from the ADP form (Figure 9B).

As shown by Beinker et al., NBD2-C-catalyzed hydrolysis of ATP under single-turnover conditions can be described by two exponential functions with rate constants of 3.5 and 0.1 s^{-1}. If we compare this hydrolysis rate to the dissociation rate constant of ADP (1.2 s^{-1}), then we should see a fluorescence increase arising from a steady state ADP occupancy at NBD2-C as the fast hydrolysis rate is 3 times faster than the exchange rate. However, as discussed above, we are mainly observing binding to the monomeric form of NBD2-C which is assumed to have less ATPase activity (if at all), so we do not spectroscopically observe phases associated with ATP hydrolysis.

Our detailed characterization of NBD2-C nucleotide binding provides a model system for the nucleotide binding properties of AAA+ domains. In contrast to full-length ClpB, NBD2-C does

not assemble into higher-order oligomers but rather displays an equilibrium between monomers and dimers, which is a much simpler system to study. The fact that this construct exhibits ATPase activity in isolation shows that key features of the AAA+ active site remained functional. Because of the simplicity of the system, we could analyze our data more easily and detect possible complications such as MANT-ADP isomerization or effects due to ADP/ATP competition. The system can now be used not only to study the influence of important amino acids on nucleotide binding kinetics and hydrolysis but also to provide the basis for the study of the more complex system of full-length ClpB, which then contains two nucleotide binding domains on protomers that assemble into multimeric complexes. With our modular approach, we were able to assign the nucleotide exchange phase directly to NBD2. Interestingly, MANT-dADP binding is modulated upon complex formation, and the nucleotide exchange rate is accelerated by a factor of 4. The measured rate constants of the reconstituted system of NBD1-M (residues 141−519) and NBD2-C (residues 519−854) are in good agreement with those of full-length wild-type ClpB. But what are the molecular events that cause the modulation of MANT-dADP binding? One characteristic feature of ClpB and Hsp104 is the C-terminal domain that follows NBD2. Previous work has shown that this domain is involved in oligomerization (*14*, *42*) and that it also contains the sensor 2 arginine that participates in nucleotide binding (*29*, *32*). The C-terminal domain could couple oligomerization to nucleotide binding. Binding of ADP to full-length $ClpB_{Th}$ causes dissociation of the complex into smaller oligomers (*10*), yet we could show that incorporation of NBD2-C into a multimeric complex increases the dissociation rate constant several-fold. It is not clear whether ADP-induced dissociation of $ClpB_{Th}$ has a function per se or whether ADP binding induces an important conformation of the ATP cycle with weaker contacts of the domains as shown by cryo-electron microscopy reconstructions (*43*), but it would be interesting to elucidate the role of the C-terminal domain in coupling oligomerization to nucleotide binding, since this could be an important domain cross talk in the regulation and coordination of the ClpB ATPase cycle.

ACKNOWLEDGMENT

We thank Jessica Eschenbach for skilled technical assistance with the HPLC analysis, molecular biology, and protein purification and Marie Rethagen, Melanie Weisser, and Sabine Zimmermann for excellent technical support with molecular biology and protein purification. We thank Robert Shoeman for support and expertise in analytical ultracentrifugation experiments, Petr Kuzmic for fruitful discussions and constant support for numerical analyses using Dynafit, and Phillip Beinker for designing and generating the initial NBD1 and NBD2 constructs. We also thank John Wray and Thorsten Lorenz for stimulating discussions and constructive criticism and the anonymous reviewers for helpful comments on the manuscript. J.R. is member of the Cluster of Excellence CellNetworks, Heidelberg.

REFERENCES

1. Frohlich, K. U. (2001) An AAA family tree. *J. Cell Sci. 114*, 1601–1602.
2. Lupas, A. N., and Martin, J. (2002) AAA proteins. *Curr. Opin. Struct. Biol. 12*, 746–753.
3. Schirmer, E. C., Glover, J. R., Singer, M. A., and Lindquist, S. (1996) HSP100/Clp proteins: A common mechanism explains diverse functions. *Trends Biochem. Sci. 21*, 289–296.
4. Doyle, S. M., and Wickner, S. (2009) Hsp104 and ClpB: Protein disaggregating machines. *Trends Biochem. Sci. 34*, 40–48.
5. Weibezahn, J., Schlieker, C., Tessarz, P., Mogk, A., and Bukau, B. (2005) Novel insights into the mechanism of chaperone-assisted protein disaggregation. *Biol. Chem. 386*, 739–744.
6. Glover, J. R., and Lindquist, S. (1998) Hsp104, Hsp70, and Hsp40: A novel chaperone system that rescues previously aggregated proteins. *Cell 94*, 73–82.
7. Lee, S., Choi, J. M., and Tsai, F. T. (2007) Visualizing the ATPase cycle in a protein disaggregating machine: Structural basis for substrate binding by ClpB. *Mol. Cell 25*, 261–271.
8. Wendler, P., Shorter, J., Plisson, C., Cashikar, A. G., Lindquist, S., and Saibil, H. R. (2007) Atypical AAA+ subunit packing creates an expanded cavity for disaggregation by the protein-remodeling factor Hsp104. *Cell 131*, 1366–1377.
9. Hattendorf, D. A., and Lindquist, S. L. (2002) Cooperative kinetics of both Hsp104 ATPase domains and interdomain communication revealed by AAA sensor-1 mutants. *EMBO J. 21*, 12–21.
10. Schlee, S., Groemping, Y., Herde, P., Seidel, R., and Reinstein, J. (2001) The chaperone function of ClpB from *Thermus thermophilus* depends on allosteric interactions of its two ATP-binding sites. *J. Mol. Biol. 306*, 889–899.
11. Schirmer, E. C., Ware, D. M., Queitsch, C., Kowal, A. S., and Lindquist, S. L. (2001) Subunit interactions influence the biochemical and biological properties of Hsp104. *Proc. Natl. Acad. Sci. U.S.A. 98*, 914–919.
12. Werbeck, N. D., Schlee, S., and Reinstein, J. (2008) Coupling and dynamics of subunits in the hexameric AAA+ chaperone ClpB. *J. Mol. Biol. 378*, 178–190.
13. Beinker, P., Schlee, S., Groemping, Y., Seidel, R., and Reinstein, J. (2002) The N terminus of ClpB from *Thermus thermophilus* is not essential for the chaperone activity. *J. Biol. Chem. 277*, 47160–47166.
14. Mogk, A., Schlieker, C., Strub, C., Rist, W., Weibezahn, J., and Bukau, B. (2003) Roles of individual domains and conserved motifs of the AAA+ chaperone ClpB in oligomerization, ATP hydrolysis, and chaperone activity. *J. Biol. Chem. 278*, 17615–17624.
15. Beinker, P., Schlee, S., Auvula, R., and Reinstein, J. (2005) Biochemical coupling of the two nucleotide binding domains of ClpB: Covalent linkage is not a prerequisite for chaperone activity. *J. Biol. Chem. 280*, 37965–37973.
16. Hiratsuka, T. (1983) New ribose-modified fluorescent analogs of adenine and guanine nucleotides available as substrates for various enzymes. *Biochim. Biophys. Acta 742*, 496–508.
17. Talavera, M. A., and De La Cruz, E. M. (2005) Equilibrium and kinetic analysis of nucleotide binding to the DEAD-box RNA helicase DbpA. *Biochemistry 44*, 959–970.
18. Schuck, P. (2000) Size-distribution analysis of macromolecules by sedimentation velocity ultracentrifugation and Lamm equation modeling. *Biophys. J. 78*, 1606–1619.
19. Akoev, V., Gogol, E. P., Barnett, M. E., and Zolkiewski, M. (2004) Nucleotide-induced switch in oligomerization of the AAA+ ATPase ClpB. *Protein Sci. 13*, 567–574.
20. Eccleston, J. F., Moore, K. J., Brownbridge, G. G., Webb, M. R., and Lowe, P. N. (1991) Fluorescence approaches to the study of the p21ras GTPase mechanism. *Biochem. Soc. Trans. 19*, 432–437.
21. Cheng, J. Q., Jiang, W., and Hackney, D. D. (1998) Interaction of mant-adenosine nucleotides and magnesium with kinesin. *Biochemistry 37*, 5288–5295.
22. Rensland, H., Lautwein, A., Wittinghofer, A., and Goody, R. S. (1991) Is there a rate-limiting step before GTP cleavage by H-ras p21?. *Biochemistry 30*, 11181–11185.
23. Bujalowski, W., and Jezewska, M. J. (2000) Kinetic mechanism of nucleotide cofactor binding to *Escherichia coli* replicative helicase DnaB protein. Stopped-flow kinetic studies using fluorescent, ribose-, and base-modified nucleotide analogues. *Biochemistry 39*, 2106–2122.
24. Vineyard, D., Zhang, X., and Lee, I. (2006) Transient kinetic experiments demonstrate the existence of a unique catalytic enzyme form in the peptide-stimulated ATPase mechanism of *Escherichia coli* Lon protease. *Biochemistry 45*, 11432–11443.
25. Jeong, Y. J., Kim, D. E., and Patel, S. S. (2004) Nucleotide binding induces conformational changes in *Escherichia coli* transcription termination factor Rho. *J. Biol. Chem. 279*, 18370–18376.
26. Rodnina, M. V., Fricke, R., Kuhn, L., and Wintermeyer, W. (1995) Codon-dependent conformational change of elongation factor Tu preceding GTP hydrolysis on the ribosome. *EMBO J. 14*, 2613–2619.
27. Woodward, S. K., Eccleston, J. F., and Geeves, M. A. (1991) Kinetics of the interaction of 2′(3′)-O-(N-methylanthraniloyl)-ATP with myosin subfragment 1 and actomyosin subfragment 1: Characterization of two acto-S1-ADP complexes. *Biochemistry 30*, 422–430.

28. Thomä, N., and Goddy, R. S. (2003) What to do if there is no signal: Using competition experiments to determine binding parameters. In Kinetic Analysis of Macromolecules: A Practical Approach (Johnson, K., Ed.) pp 153−170, Oxford University Press, New York.
29. Hattendorf, D. A., and Lindquist, S. L. (2002) Analysis of the AAA sensor-2 motif in the C-terminal ATPase domain of Hsp104 with a site-specific fluorescent probe of nucleotide binding. *Proc. Natl. Acad. Sci. U.S.A. 99*, 2732–2737.
30. Ghanem, M., Li, L., Wing, C., and Schramm, V. L. (2008) Altered thermodynamics from remote mutations altering human toward bovine purine nucleoside phosphorylase. *Biochemistry 47*, 2559–2564.
31. Groemping, Y., and Reinstein, J. (2001) Folding properties of the nucleotide exchange factor GrpE from *Thermus thermophilus*: GrpE is a thermosensor that mediates heat shock response. *J. Mol. Biol. 314*, 167–178.
32. Lee, S., Sowa, M. E., Watanabe, Y. H., Sigler, P. B., Chiu, W., Yoshida, M., and Tsai, F. T. (2003) The structure of ClpB: A molecular chaperone that rescues proteins from an aggregated state. *Cell 115*, 229–240.
33. Erzberger, J. P., and Berger, J. M. (2006) Evolutionary relationships and structural mechanisms of AAA+ proteins. *Annu. Rev. Biophys. Biomol. Struct. 35*, 93–114.
34. Burton, R. E., Baker, T. A., and Sauer, R. T. (2003) Energy-dependent degradation: Linkage between ClpX-catalyzed nucleotide hydrolysis and protein-substrate processing. *Protein Sci. 12*, 893–902.
35. Yakamavich, J. A., Baker, T. A., and Sauer, R. T. (2008) Asymmetric nucleotide transactions of the HslUV protease. *J. Mol. Biol. 380*, 946–957.
36. Leskovar, A., and Reinstein, J. (2008) Photophysical properties of popular fluorescent adenosine nucleotide analogs used in enzyme mechanism probing. *Arch. Biochem. Biophys. 473*, 16–24.
37. Fersht, A. (1998) Structure and mechanism in protein science , W. H. Freeman, New York.
38. Licht, S., and Lee, I. (2008) Resolving individual steps in the operation of ATP-dependent proteolytic molecular machines: From conformational changes to substrate translocation and processivity. *Biochemistry 47*, 3595–3605.
39. Hersch, G. L., Burton, R. E., Bolon, D. N., Baker, T. A., and Sauer, R. T. (2005) Asymmetric interactions of ATP with the AAA+ ClpX6 unfoldase: Allosteric control of a protein machine. *Cell 121*, 1017–1027.
40. Goldberg, A. L., Moerschell, R. P., Chung, C. H., and Maurizi, M. R. (1994) ATP-dependent protease La (lon) from *Escherichia coli*. *Methods Enzymol. 244*, 350–375.
41. Schlee, S., Beinker, P., Akhrymuk, A., and Reinstein, J. (2004) A chaperone network for the resolubilization of protein aggregates: Direct interaction of ClpB and DnaK. *J. Mol. Biol. 336*, 275–285.
42. Mackay, R. G., Helsen, C. W., Tkach, J. M., and Glover, J. R. (2008) The C-terminal extension of *Saccharomyces cerevisiae* Hsp104 plays a role in oligomer assembly. *Biochemistry 47*, 1918–1927.
43. Wendler, P., Shorter, J., Snead, D., Plisson, C., Clare, D. K., Lindquist, S., and Saibil, H. R. (2009) Motor mechanism for protein threading through Hsp104. *Mol. Cell 34*, 81–92.